Tectonics

Late Paleozoic Iberian Orocline(s) and the Missing Shortening in the Core of Pangea. Paleomagnetism From the Iberian Range

Daniel Pastor-Galán[1,2] (iD), Emilio L. Pueyo[3], Mark Diederen[2], Cristina García-Lasanta[4] (iD), and Cor G. Langereis[2] (iD)

[1]CNEAS, Tohoku University, Sendai, Japan, [2]Faculty of Geosciences, Utrecht University, Utrecht, The Netherlands, [3]Instituto Geológico y Minero de España, Unidad de Zaragoza, Zaragoza, Spain, [4]Universidad de Zaragoza, Zaragoza, Spain

Abstract Supercontinents are usually interpreted to be single and rigid continental plates. How and when Pangea became a rigid supercontinent is disputed, and age estimations vary from ~330 to ~240 Ma. The Gondwana-Laurussia collision formed the Variscan-Alleghanian belt, the most prominent witness of Pangea's amalgamation. In Iberia, this orogen draws an "S" shape featured by the Cantabrian Orocline and the Central Iberian curve. The curvature of Central Iberia is particularly evident in Galicia-Trás-os-Montes and in a change of trend that it draws in the Aragonese Branch of the Iberian Range. Recent research showed that both curvatures are not coeval and that the Central Iberian curve had to form prior to ca. 318 Ma (i.e., not a secondary orocline). We report paleomagnetic and structural results from Paleozoic rocks in the Santa Cruz syncline (Aragonese Branch of the Iberian Range) that indicate two main vertical axis rotations events: (1) a Cenozoic (Alpine) clockwise rotation of >20° and (2) a late Carboniferous counterclockwise rotation of ~70°. Once the Cenozoic rotation is restored, the change in structural trend that allegedly evidences the outer arc of the Central Iberian curve disappears. Whereas the Cenozoic rotation is incompatible with a Central Iberian curve, the late Carboniferous rotation is fully compatible with the Cantabrian Orocline, enlarging the area affected by its counterclockwise rotations and the existence of a nonrigid Pangea until, at least, ~295 Ma.

Plain Language Summary Supercontinents like Pangea are thought to be rigid and stable in its interiors. It is not clear, however, when the supercontinents achieve its final rigid and sturdy form. There is a debate on when Pangea became a rigid supercontinent; some people argue that it happened as soon as 330 million years ago and others as recently as 240. The Iberian peninsula witnessed all this process, and today, we still can see the relic of the mountain range formed at that time with an "S" shape. Recent research showed that both north and south curvatures did not form coevally and that the southern curve formed before 318 Ma. We report paleomagnetic and structural results from Paleozoic rocks in the Aragonese Branch of the Iberian Range that indicate that the change in trend that allegedly evidences the southern curve of this "S" shape is a much later effect of Alpine tectonics. Altogether, the results show that Pangea was not rigid until at least 290 million years ago.

1. Introduction

Supercontinents are interpreted to be single continental plates of a size capable of influencing mantle convection patterns and even core-mantle boundary processes (Pastor-Galán, Nance, et al., 2018). The amalgamation and breakup of Pangea, the latest supercontinent, are the geologists' template for the supercontinent cycle today. Whereas the configuration of Pangea during its breakup is well constrained due to the preservation of ocean floor from the Jurassic to the present (e.g., Seton et al., 2012), its amalgamation history is less certain and our only evidence is carved in the Paleozoic geological record. Controversy remains about the continental configuration of Pangea during its amalgamation (cf. Pangea A, B, C hypotheses; Belica et al., 2017; Domeier et al., 2012; Gallo et al., 2017), the number of participating continents, and their kinematic evolution during the Paleozoic (e.g., Domeier & Torsvik, 2014; Stampfli et al., 2013). Very importantly, there is a large and ongoing debate on when Pangea became a genuine supercontinent with contrasting age estimations ranging between ~330 and ~240 Ma (e.g., Blakey & Ranney, 2018; Veevers, 2004).

The most important event in Pangea assemblage was the Late Paleozoic collision between Gondwana, Laurussia (Laurentia + Baltica + Avalonian-Megumian terranes), and several microplates (Nance et al., 2010) resulting in the sinuous Variscan-Alleghanian orogen, which swirls several times from Bohemia to Alabama. Two of these orogenic curves are located in the Iberian Peninsula, drawing an "S" shape: (1) the Cantabrian Orocline (e.g., Gutiérrez-Alonso et al., 2012) to the north and (2) the Central Iberian curve to the south (e.g., Aerden, 2004). In this paper we use the term *orocline* strictly in its kinematic definition: The curvature of an orocline is a product of vertical axis rotations (Johnston et al., 2013). The Cantabrian Orocline twists the Variscan trend from Brittany across the Bay of Biscay to enter into Central Iberia, and its geometry is especially obvious in its core in NW Iberia (e.g., Weil et al., 2013). The Cantabrian Orocline formed by vertical axis rotations and is kinematically well constrained: It developed from Moscovian to Asselian times (~310–295 Ma; e.g., Pastor-Galán et al., 2011; Weil et al., 2010). The geometry of the Central Iberian curve is, however, much less constrained due to limited exposures. Some authors claim that the changes in trend observed in the Galicia-Trás-os-Montes Zone (West Iberia), the eastern most area of the Central Iberian Zone and the Aragonese Branch of the Iberian Range (Figure 1) correspond with a syn-Variscan or post-Variscan orogeny orocline formation (e.g., Martínez Catalán, 2012; Shaw et al., 2012). From a kinematic point of view, the Central Iberian curve must have formed prior to ca. 318 Ma (Pastor-Galán et al., 2016), at least in West Iberia. It is not known, however, whether its formation involved vertical axis rotations and, if so, to what extent. The kinematics of the Cantabrian Orocline and the potentially expected vertical axis rotations in the Central Iberian curve require significant amounts of shortening and extension yet to be quantified and included in global reconstructions.

In this paper, we use paleomagnetism in the Santa Cruz de Nogueras syncline (Aragonese Branch of the Iberian Range) to study the kinematic history and involvement of the Iberian Range in the Central Iberian curve. Our results confirm the intracontinental deformation Pangea had to undergo to accommodate the late Carboniferous and Early Permian vertical axis rotations in the Variscan Belt.

2. Tectonic and Geological Settings

2.1. Tectonic and Paleogeographic Background

After the Late Silurian–Early Devonian collision between Avalonia (s.l.), Baltica, and Laurentia had formed the Appalachian-Caledonide orogeny (e.g., Domeier, 2016; Mac Niocaill, 2000; van Staal et al., 2009), the closure of the Rheic Ocean started (e.g., Bozkurt et al., 2008; Nance et al., 2010). Subduction of the Rheic Ocean was followed by the collision between Laurussia and Gondwana and several microplates, which formed the Variscan-Alleghanian-Ouachita belt that seamed Pangea, at the end of the Carboniferous (e.g., Domeier and Torsvik, 2014; Stampfli et al., 2013).

Variscan deformation in Iberia commenced at ca. 400 Ma (e.g., Gómez Barreiro et al., 2006), although the first evidence of continental collision dates from ca. 365 to 370 Ma (e.g., Dallmeyer et al., 1997; López-Carmona et al., 2014) with the underplating of the Gondwanan margin below Laurussia (e.g., Pérez-Cáceres et al., 2015; Pereira, Gutíerrez-Alonso, et al., 2017). Deformation, metamorphism, magmatic episodes, and synorogenic sedimentation migrated east-northeastward (in present-day coordinates) progressively toward the foreland (e.g., Dallmeyer et al., 1997) where shortening commenced at approximately 325 Ma (e.g., Pérez-Estaún et al., 1991).

The Iberian Variscides depict a sinuous "S-shaped" geometry of two opposing first-order magnitude bends (Figure 1a) delineated by the well-known Cantabrian Orocline to the north and the Central Iberian curve to the south. Orogenic bends are classified based on the kinematics of their curvature development (e.g., Johnston et al., 2013). Correlations between changes in the structural grain and paleomagnetic directions or rock fabrics are evaluated using an orocline test (e.g., Pastor-Galán, Gutiérrez-Alonso, et al., 2017; Pastor-Galán, Mulchrone, et al., 2017, and references therein), which distinguishes two end-members: (1) primary bends, showing a slope (m) = 0, and (2) secondary oroclines, with m = 1. Intermediate relations ($0 < m < 1$) are known as progressive oroclines.

The Cantabrian Orocline (a.k.a. Cantabrian Arc and Cantabria-Asturias Arc) formed as a late orogenic feature in a short period of 10 to 15 Myr between ~310 and ~295 Ma (Pastor-Galán et al., 2011; Weil et al.,
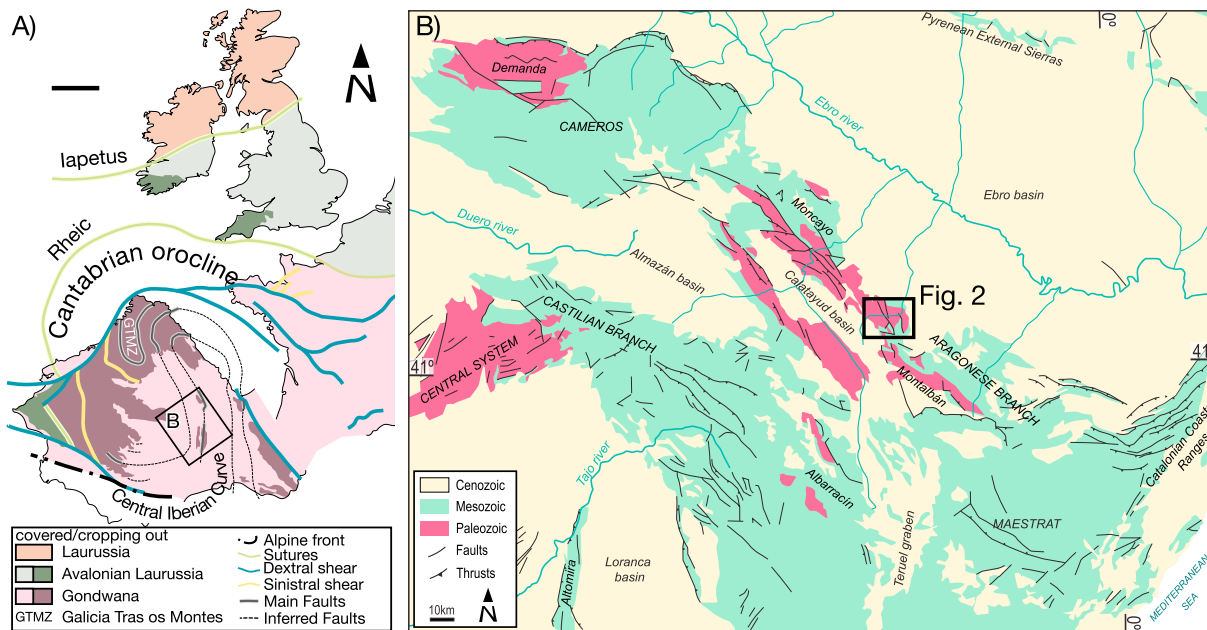
Figure 1. a) Location of the main Variscan orogeny outcrops in western Europe with Iberia restored to a pre-Albian rotation (Gong et al., 2008). We highlight the Galicia-Trás-os-Montes Zone, the Iberian Range, and the eastern Central Iberian Zone to remark the areas where the Central Iberian curve is more evident. (b) Simplified geological map of the Iberian Range after García-Lasanta et al. (2017), highlighting the Paleozoic outcrops and the studied area.

2013). Its structural trend traces a curvature that runs from Brittany across the Bay of Biscay passing through South England and Ireland into Central Iberia (Figure 1a; Pastor-Galán, Ursem, et al., 2015), and its geometry is evident from satellite imagery, especially at its core. Many paleomagnetic and geological studies support the Cantabrian Orocline as secondary feature (e.g., Weil et al., 2013, and references therein). Widespread mantle-derived magmatism occurred coeval with the Cantabrian Orocline formation (between ~312 and ~290 Ma; Gutiérrez-Alonso, Fernández-Suárez, et al., 2011; Gutiérrez-Alonso, Murphy, et al., 2011; Pastor-Galán, Gutiérrez-Alonso, Mulchrone, et al., 2012; Pereira et al., 2014, 2015; Pereira, Gama, et al., 2017; Weil et al., 2013).

Described for the first time by Staub (1926), the Central Iberian curve turns the Variscan orogen concave to the west immediately to the south of the Cantabrian Orocline (Figure 1). In contrast with the Cantabrian Orocline, the geometry and kinematics of the Central Iberian curve are poorly understood and were over-looked for decades due to poor exposure (Martínez Catalán et al., 2015). The observations used in support of the Central Iberian curved geometry are as follows: (1) paleocurrents recorded in Ordovician quartzites (Shaw et al., 2012); (2) fold trends and inclusions in garnets (Aerden, 2004), and (3) fold trends and aeromagnetic anomalies (Martínez Catalán, 2012). Based on these arguments, authors have suggested three competing geometries (Pastor-Galán, Groenewegen, et al., 2015), which differ in the amount of orogenic curvature, from a maximum of 180° (Shaw et al., 2012) to the no more than 100° (Martínez-Catalán, 2011). All of them, however, share two features in common: (1) the curvature encloses the center-west of Iberia with Galicia-Trás-os-Montes Zone in the core (Aerden, 2004; Pastor-Galán, Dias da Silva, et al., 2018) and (2) the change in trend in the outer arc is primarily marked by the outcrops in the Aragonese Branch of the Iberian Range and eastern Central Iberian Zone (Martínez Catalán, 2012).

Paleomagnetic results from the core and southern limb of the Central Iberian curve show an overall rotation that fits with the attitude of the southern limb of the Cantabrian Orocline (Pastor-Galán, Groenewegen, et al., 2015; Pastor-Galán et al., 2016; Pastor-Galán, Gutiérrez-Alonso, et al., 2017; Pastor-Galán, Mulchrone, et al., 2017). However, the timing constraints provided by these results established that no differential rotation occurred younger than ca. 318 Ma, and therefore, if the Central Iberian curve is oroclinal, then it must have become secondarily curved prior to ~318 Ma (Pastor-Galán, Gutiérrez-Alonso, et al., 2017; Pastor-Galán, Mulchrone, et al., 2017).
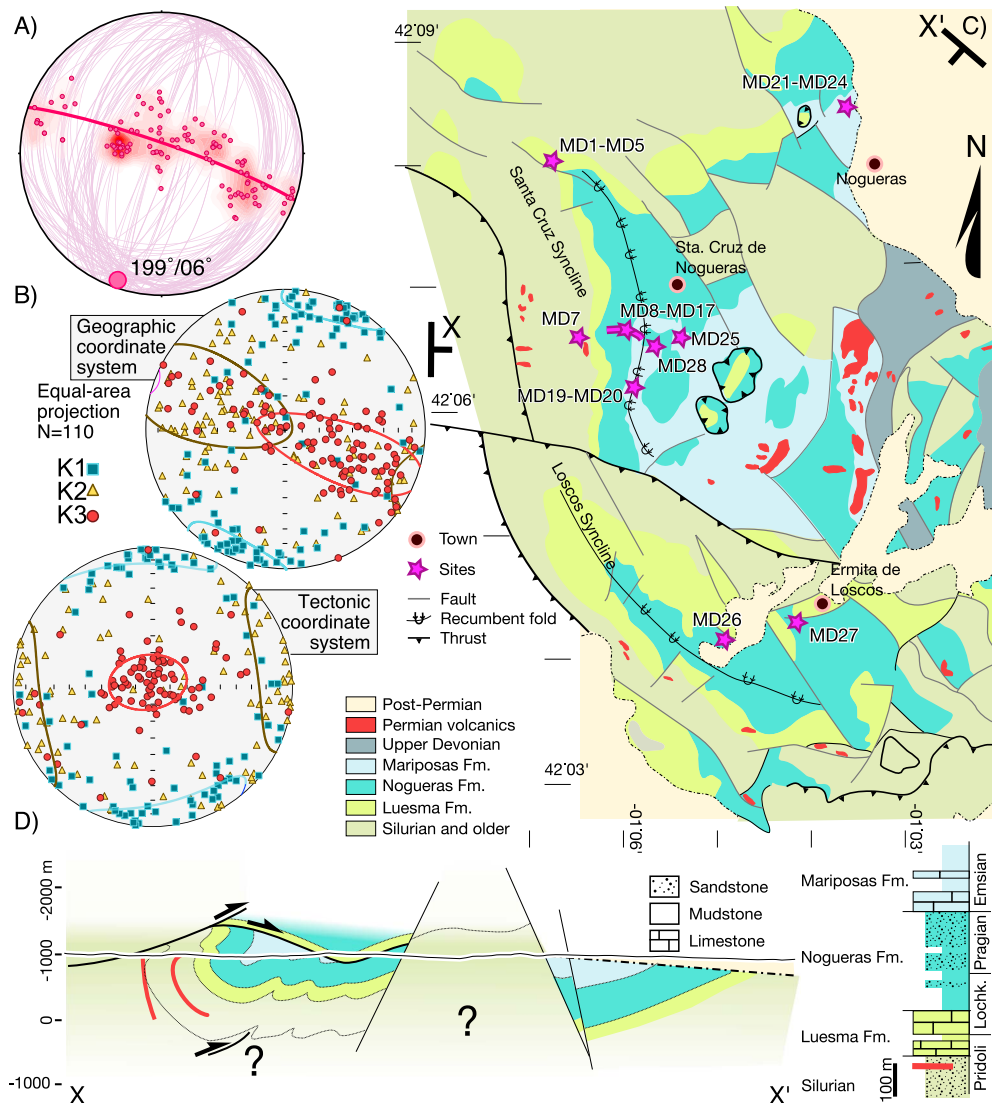
Figure 2. Structure and lithology of the Santa Cruz syncline. (a) Pi diagram showing all the bedding measurements taken and the fold axis attitude. (b) Anisotropy of magnetic susceptibility fabrics showing a sedimentary magnetic fabric (k_3 is perpendicular to bedding) with a slight tectonic fabric (k_1 is subparallel to the fold axis). (c) Geological map of the studied area and location of the samples collected. (d) Cross-section through the Santa Cruz syncline and synthetic stratigraphy of the Santa Cruz syncline sampling area.

2.2. Geological Setting

The Variscan orogen is classically divided into a number of tectonostratigraphic zones based on fundamental differences in their stratigraphic, structural, magmatic, and metamorphic evolution (e.g., Ballèvre et al., 2014). The Cantabrian Zone contains an almost complete stratigraphy spanning from Ediacaran to Early Permian and represents the foreland fold-and-thrust belt of the Variscan orogen (Pérez-Estaún et al., 1990). Structurally, it is characterized by tectonic transport toward the core of the orocline, low finite strain values, and locally developed cleavage (e.g., Kollmeier et al., 2000; Pastor-Galán et al., 2009; Pérez-Estaún et al., 1991). Illite crystallinity and conodont color alteration indexes are consistent with diagenetic conditions to very low grade metamorphism (e.g., García-López et al., 2013; Pastor-Galán et al., 2013). The Cantabrian Zone is mostly preserved in NW Iberia in the core of the Cantabrian Orocline (Figure 1a; Pastor-Galan, Gutierrez-Alonso, Zulauf, et al., 2012), but it also crops out in areas of the Aragonese Branch of the Iberian Range in East Iberia (Figure 1b; Calvín-Ballester & Casas-Sainz, 2014; Carls, 1983, 1988), where we performed our study (Figures 1b and 2).

The Iberian Range (Figure 1b) formed in response to the intraplate deformation triggered by the Alpine orogeny in the eastern central part of the Iberian Peninsula during the Cenozoic (e.g., Alvaro et al., 1978; Casas-Sainz & Faccena, 2001; Cortes Gracia & Casas-Sáinz, 1996). It is configured in two main branches trending mainly NW–SE: the Aragonese Branch (northward) and the Castilian Branch (southward). Our study focuses on one of the two elongated Paleozoic units that crop out in the central part of the Aragonese branch (Figure 1). Paleozoic rocks in the studied area are structured into two tectonostratigraphic units: Badules and Herrera. Whereas the Herrera unit is the continuation of the foreland (Cantabrian Zone), the Badules unit represents more internal zones of the orogen (e.g., Gozalo & Liñan, 1988). The Herrera Unit preserves over 9,000-m-thick sedimentary sequence containing a Cambrian–Silurian alternation of sandstones and shales and, over it, the studied Upper Silurian–Devonian series of shales, sandstones, and limestones (Luesma, Nogueras, and Mariposas Formations; Figure 2; Calvín-Ballester & Casas-Sainz, 2014; Pérez-Pueyo et al., 2018, and references therein) that crop out at the south of the unit (Figures 1b and 2). The Herrera unit is characterized by an imbricate thrust system with a foreland-dipping geometry in which the deformation and cleavage diminishes eastward (Calvin et al., 2014). Silurian to Devonian rocks crop out in two overturned synclines with NNW–SSE to NW–SE trend (Figure 2): Santa Cruz and Loscos. Early Permian mantle-derived magmatism intruded the Herrera unit, and the igneous rocks occur as effusive, subvolcanic dykes and sills and minor plutons (e.g., Calvin et al., 2014, and references therein). A series of 1,500-m-thick Mesozoic sedimentary series (Calvin et al., 2014) overlies the Herrera and Badules Paleozoic units. Both sequences underwent gentle folding during the Alpine compression event with no associated penetrative structures (Cortes Gracia & Casas-Sáinz, 1996).

The present outcrop of Paleozoic basement rocks in the Iberian Range is strongly conditioned by subsequent Late Paleozoic-Mesozoic rifting episodes, the later inversion of those basins during the Alpine deformation in Cenozoic times, and a final extensional event during the Neogene (Salas & Casas, 1993). Two major rifting events took place during Late Permian–Triassic and during Late Jurassic–Early Cretaceous controlled by major Variscan anisotropies, and main depocenters were located northwest and southeast of the study area. Subsequent Alpine deformation inverted the previous extensional basins and produced a fold-and-thrust belt displaying interference geometries, strike and reverse-slip movements, and complex thin-skinned/thick-skinned relationships (de Vicente et al., 2009; Guimerà et al., 2004; Salas et al., 2001; E. Izquierdo-Llavall et al., personal communication, 2018). Finally, a Neogene NW-SE extension related to the opening of the Mediterranean western basins led to the final configuration of the Iberian Range system (Roca & Guimerà, 1992; Simón Gómez, 1982).

Previous paleomagnetic studies in Permian (dolerites) and Mesozoic (limestones) rocks in the region have reported primary Permian and Oxfordian components (Calvin et al., 2014; Juárez et al., 1994, respectively) as well as Lower Cretaceous remagnetizations (Gong et al., 2008; Juárez et al., 1998). However, reported declinations of all these results should be used with caution since recent data from younger Triassic to Eocene sedimentary cover confirmed the occurrence of clockwise (CW) rotations related to Alpine compression (H. J. Mauritsch et al., personal communication, 2018). Following these authors, the mean Cenozoic paleomagnetic direction in the Central Iberian Range was Dec./Inc. = 025°/57° (k = 35.4) which yields a consistent 21° CW rotation with respect to the Cenozoic reference direction for Iberia (Dec./Inc. = 004°/46°; k = 110.6). In addition, the paleomagnetic results are supported by shortening differences along strike found after the restoration of balanced cross-sections in the region (E. Izquierdo-Llavall et al., personal communication, 2018).

3. Methods and Results

We drilled a total of 300 cores from 28 sites with a petrol engine drill and took over 100 structural orientations (Figure 2 and Table 1; supporting information Figure S1 for exact location) in the Silurian and Devonian sedimentary series including clastic (sandstones and mudstones) and carbonates that crop out to the south of the Herrera unit at the Aragonese Branch of the Iberian Range, as well as Permian subvolcanic dolerites (MD7 and MD21; Figures 1 and 2). We performed all analyses at Paleomagnetic Laboratory Fort Hoofddijk, Universiteit Utrecht, The Netherlands.

3.1. Structure and Anisotropy of the Magnetic Susceptibility

The Santa Cruz syncline is a nearly recumbent cylindrical fold with a nonplunging axis that swings from NW-SE to NNE–SSW trend (Figure 2a). We collected most of the samples in the area where the trend is NNE–SSW and obtain an average value of Trend = 199°and Plunge = 6° (Figure 2a). In the studied area

Table 1
Paleomagnetic Results and Statistical Information for Each Component

Composition	N_s	N_{45}	Dec	Inc	k	α_{95}	K	A_{95min}	A_{95}	A_{95max}	ΔDx	ΔIx	λ
#1 (Geo)	49	49	**150.4**	**8.3**	**15.5**	**5.3**	**29**	2.5	< 3.8	< 7.1	3.9	7.6	−4.2
#1 (TC)	49	36	155.6	21.0	11.9	7.2	24	2.9	< 5.0	< 8.6	5.1	9.0	−10.9
#2 (Geo)	46	32	118.5	11.4	8.2	9.4	11.3	3.0	< 7.9	< 9.2	7.9	15.3	−5.8
#2 (TC)	46	46	**107.3**	**12.7**	**8.0**	**7.9**	**13**	2.6	< 6.1	< 7.3	6.1	11.7	−6.4
P (Geo)	104	104	**183.2**	**4.5**	**17.6**	**3.4**	**35.8**	1.9	< 2.3	< 4.4	2.4	4.7	−2.2
P (TC)	104	99	193.1	−17.6	11.8	4.3	16	1.9	< 3.7	< 4.5	3.7	6.8	9.0
P Dykes	31	31	191.3	−8.8	35.3	4.4	55.5	3.0	< 3.5	< 9.4	3.5	6.9	4.4
P-All	135	135	**185.1**	**1.4**	**17.8**	**3.0**	**34.8**	1.7	< 2.1	< 3.7	2.1	4.2	−0.7

Note. Values in bold are the results used in the paper.

little to no penetrative microfabrics and mesofabrics developed, and strain patterns based on field constraints are limited to thrusts and folds.

Anisotropy of magnetic susceptibility (AMS) is a very sensitive method that can help in describing deformational events even in weakly deformed contexts where tectonic lineation and foliation have not developed (e.g., Mattei et al., 1997; Pares, 2015; Weil & Yonkee, 2009), and it is represented graphically as an ellipsoid whose principal axes are $k_1 > k_2 > k_3$ (Borradaile, 1988; Pares, 2015, and references therein). The shape of the AMS ellipsoid depends on the crystallographic preferred orientation of the individual components, the rock's compositional layering, distribution and size of microfractures, and the shape, size, and preferred orientation of mineral grains (e.g., Butler, 1992; Tarling & Hrouda, 1993; Tauxe, 2010). In undeformed sedimentary rocks, AMS ellipsoid usually shows an oblate geometry with its magnetic foliation plane parallel to bedding and k_3 perpendicular to it, in some occasions a lineation might develop, indicating a paleocurrent (e.g., Tarling & Hrouda, 1993). In contrast, the AMS ellipsoid in deformed rocks develops a magnetic lineation (k_1) typically representing intersection lineations in weakly deformed settings (i.e., parallel to fold axis; e.g., Oliva-Urcia et al., 2009) or maximum extension directions (e.g., Cifelli et al., 2005; García-Lasanta et al., 2015). In strongly deformed areas, the AMS ellipsoid becomes oblate again, this time with k_3 parallel to the tectonic foliation (e.g., Weil & Yonkee, 2009).

We measured the AMS of 162 samples from our Santa Cruz syncline collection with an AGICO MFK1-FA susceptometer. Samples from sites MD1 to MD7 (sedimentary and sill) and MD26 and MD27 (sedimentary) yielded no interpretable AMS results (Figure S1). The rest of the samples show triaxial AMS ellipsoids (Figures 2b and S1) but close to oblate where the most developed fabrics show k_3 perpendicular to bedding. Although k_2 and k_1 are similar, they are distinctly different; magnetic lineation (k_1) is roughly oriented to the NNE–SSW with little to no plunge and coinciding with the fold axis trend (Figure 2a), whereas k_2 is mostly parallel to the shortening direction (perpendicular to the fold axis). All these results confirm the weak deformation underwent by the studied rocks.

3.2. Paleomagnetism

We used both thermal and alternating field (AF) demagnetizations to investigate the magnetic remanence of the collected samples. AF demagnetization was carried out using a robotic 2G-SQUID magnetometer available at Utrecht University, through variable field increments (4–10 mT) up to 70–100 mT. In those samples where high-coercivity, low-blocking temperature minerals (e.g., goethite and maghemite) were expected, a preheating to 150 °C was coupled to AF demagnetization (van Velzen & Zijderveld, 1995). Stepwise thermal demagnetization was carried out in the remaining samples through 20–100 °C increments up to complete demagnetization (Figure 3 and Data Set S2). Principal component analysis (Kirschvink, 1980) was used to isolate the direction of the characteristic remanent magnetization, and results were represented by orthogonal vector endpoint demagnetization diagrams (Zijderveld, 1967) using Paleomagnetism.org (Koymans et al., 2016). Representative Zijderveld diagrams are shown in Figure 3. A minimum of five steps was considered to characterize a remanent component. In ~35 samples, two components appear to overlap; for such cases we applied the method of demagnetization great circles (Figure 3). We used the approach of McFadden and McElhinny (1988) in combining great circles and linear best fits (set points).
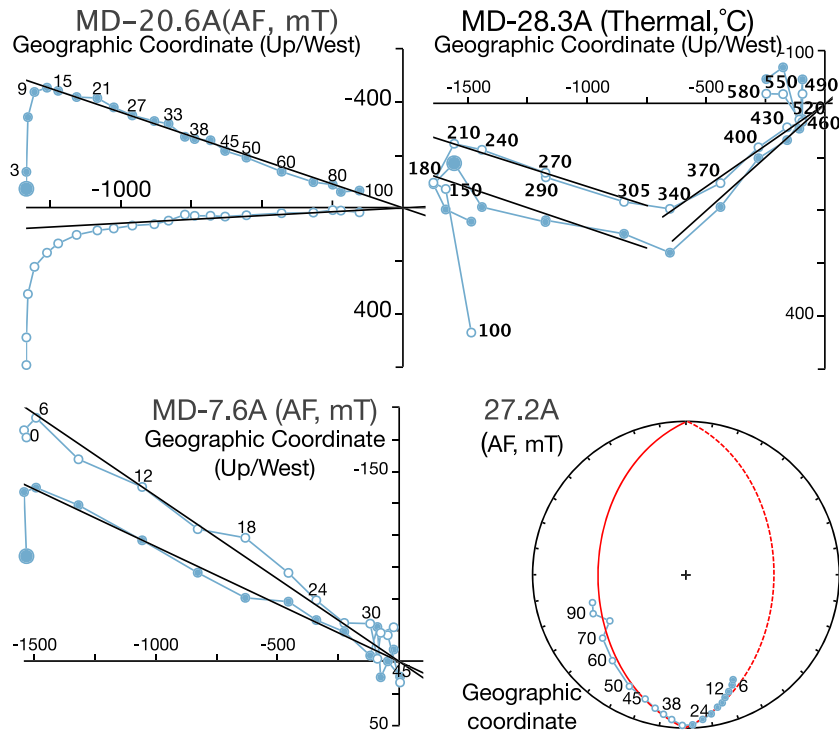
Figure 3. Representative Zijderveld diagrams and great circle approach in the studied samples. AF = alternating field.

Given the structural coherence between the studied sites and the robust paleomagnetic signal of the samples, we combined all the results in a single locality. We separated several components to which we applied a fixed 45° cut-off to their virtual geomagnetic pole (VGP) distributions (Deenen et al., 2011). Mean directions (Table 1) were evaluated using Fisher (1953) statistics of VGPs corresponding to the isolated magnetic directions, following Deenen et al. (2011). All statistics were performed with www.paleomagnetism.org (Koymans et al., 2016) and VPD software (Ramón et al., 2017). Most samples show a component that is removed at low temperatures and low coercivities (100–180 °C or 10–12 mT; Figure 3 and supporting information). We consider this component as a viscous remanent magnetization, because of its similarity to the recent field.

In addition to the viscous remanent magnetization, we have identified three components showing distinctive components:

Component P: Samples from Early Permian dykes and sills (dolerite) show a single-polarity component with southward declination and very shallow inclination (Dec./Inc. = 191.3°/−8.8°; k = 35.3, α_{95} = 4.4, K = 55.5, A_{95} = 3.5; Figure 4 and Table 1), which is consistent with that described in similar rocks in the area (Calvin et al., 2014). Component P is predominant in most of the Siluro-Devonian studied series (104 specimens) with a slightly different average of Dec./Inc. = 183.2°/4.5° (k = 17.6, α_{95} = 3.4°, K = 35.8, A_{95} = 2.3°; Table 1 and Figure 4) and a larger dispersion ($K_{sedimentary}$ = 35.8 versus $K_{igneous}$ = 55.5; Table 1). This component clusters better before any tilt correction (Table 1). When occurring together with other components, it is usually removed at 300–350° (lower T component) and over 40–50 mT (higher coercivity component). The average direction of all the samples (igneous and sedimentary) combined is Dec./Inc. = 185.1°/1.4° (k = 17.8, α_{95} = 3°, K = 34.8, A_{95} = 2.1°; Table 1).

Component #1: In 49 specimens from the Siluro-Devonian sedimentary series (Figure 2), we identified a single-polarity component heading southeast with shallow inclinations and an average direction Dec./Inc. = 150.4°/8.3° (k = 15.5, α_{95} = 5.3°, K = 29, A_{95} = 3.8°; Figure 5 and Table 1). This component does not pass a fold test (Figure 5b; Tauxe & Watson, 1994).
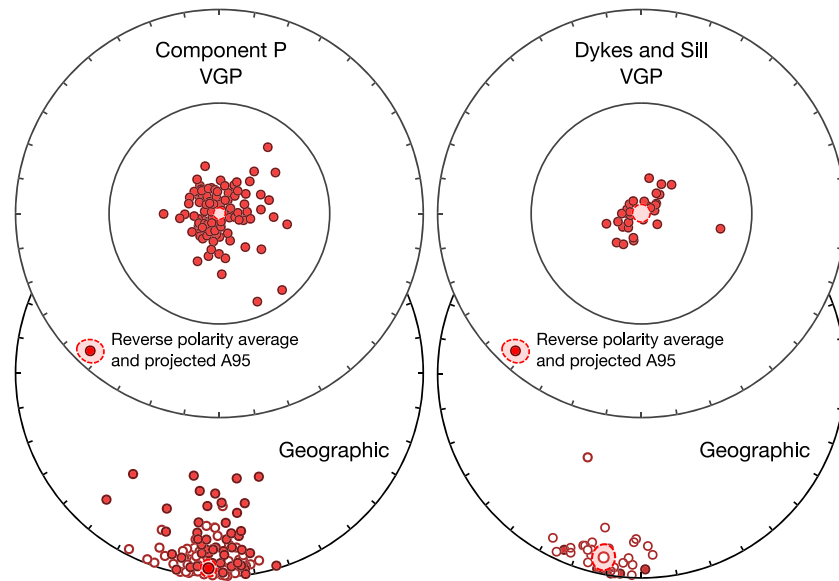
Figure 4. (left) Component P directions and virtual geomagnetic poles (VGPs) in geographic coordinates for sedimentary lithologies and (right) dykes and sill. VGPs are centered on the mean to show the shape of the distribution, ideally rounded. Note that dykes and sills show a slightly elongated distribution, likely representing a not complete average of the paleo-secular variation of the magnetic field.
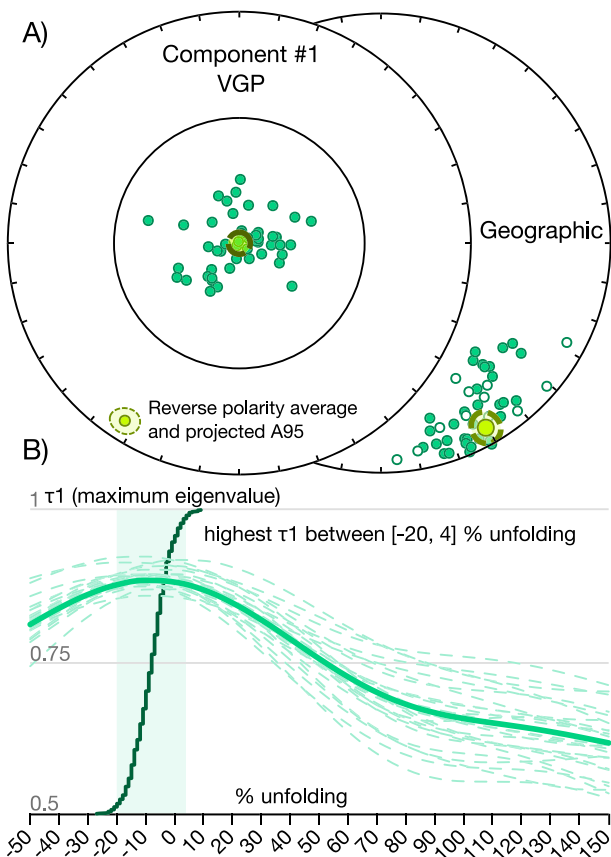

Figure 5. (a) Component #1 directions and virtual geomagnetic poles (VGPs) in geographic coordinates. (b) Negative fold test indicating the postfolding origin of the component.

Component #2: Forty-six specimens from the Siluro-Devonian sedimentary series (Figure 2) show a two-polarity component that clusters significantly better after structural correction and passes a fold test (Figure 6; Tauxe & Watson, 1994). Both polarities share a common distribution following the coordinate bootstrap test of Tauxe (2010; Figure 6). This component trends ESE–WNW and shows shallow inclinations, slightly higher than in Component #1 (average Dec./Inc. = 107.3°/12.7°; $k = 8$, $\alpha_{95} = 7.9$, $K = 13$, $A_{95} = 6.1$°; Table 1).

Demagnetization analyses and thermomagnetic runs (Data Set S2 and Figure S2, respectively) indicate that the principal magnetic carrier in dykes and sills is (Ti-poor) magnetite, as evidenced by unblocking temperatures between 480 and 580 °C and alternating magnetic fields peaks of 40–60 mT. Results from limestones and clastic rocks also point to (Ti-poor) magnetite as the main carrier of the Natural Remanent Magnetization (NRM), evidenced by maximum unblocking temperatures of 400–580 °C and alternating magnetic fields of 60–90 mT (Figure 3). The main magnetic carrier of the red limestones is hematite, demagnetizing over 600 °C and largely resistant to AF demagnetization. Some limestones show a relatively large goethite component that was fully removed at 100 °C.

4. Discussion

Unraveling the kinematics and deformational mechanisms of areas that underwent several tectonic events is a complex task that has to be solved backward in time, especially when dealing with vertical axis rotations (Pueyo et al., 2016): It is impossible to solve accurately the oldest movements without solving the youngest ones. Several authors described Alpine tectonics involving the basement units in the Iberian Range (e.g.,
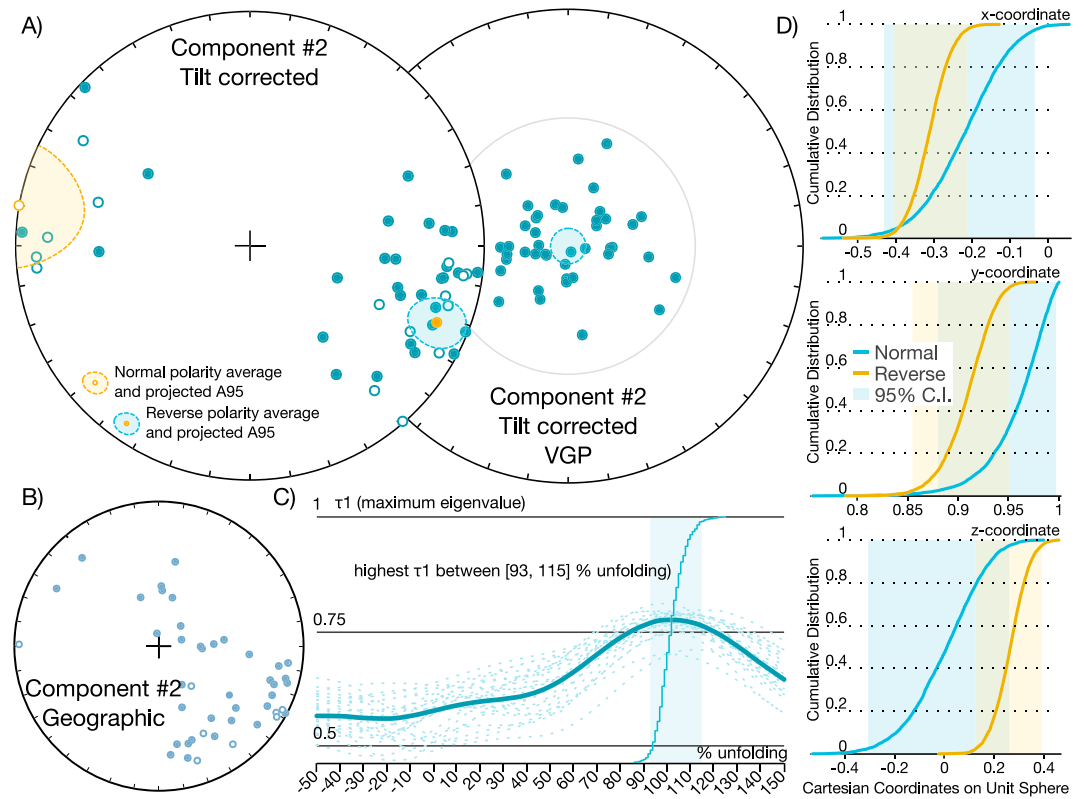
Figure 6. (a) Component #2 directions and virtual geomagnetic poles (VGPs) in structurally corrected coordinates. (b) Component #2 directions in geographic coordinates (note the high dispersion) and positive fold test, which indicates the prefolding character of this component. (c) Positive reversal test between both normal and reverse directions found in Component #2, suggesting a pre-Kiaman magnetization of the studied rocks.

E. Izquierdo-Llavall et al., personal communication, 2018). Despite the vertical axis rotations described in the area (e.g., H. J. Mauritsch et al., personal communication, 2018), the Santa Cruz syncline shows a subhorizontal axis (Figure 2a) and the Mesozoic and Cenozoic rocks overlying the Santa Cruz syncline show subhorizontal dips and no signs of refolding, thrusting, major tilting, or penetrative internal deformation (Figure 2d). These data support the fact that the particular area around the Santa Cruz syncline did not record any significant Alpine tilting.

AMS ellipsoids fit with the macrostructural data (Figures 2a and 2b). The k_3 axes are perpendicular to the bedding plane, caused by compaction after sedimentation. Despite maximum and intermediate magnetic axes distributions show a rather large dispersion; they arrange around an orientation maximum, suggesting a tectonic fabric superimposed on the sedimentary fabric. The magnetic lineation (k_1 distribution) is parallel to the Santa Cruz syncline's fold axis or, equivalently, perpendicular to the shortening direction. The structural trend (dominant N–S) as well as the overturned feature of the analyzed structures (particularly the Santa Cruz syncline) strongly differs from the expected Alpine grain (NW–SE). The AMS response and its consistency with the general macrostructure support the fact that Alpine deformation was not intense and did not trigger noticeable internal deformation in the studied lithologies. Hence and apart from rigid-body passive movements, post-Permian deformation is negligible. Absence of major internal deformation events simplifies the interpretation of Paleozoic paleomagnetic directions.

4.1. Paleomagnetism

We have identified three different magnetic components. They may occur individually or in couples (Figure 3), regardless of their lithology or structural position.

4.1.1. Component P

All Lower Permian dolerite dykes and sills (MD7 and MD21), and many of the sites sampled in Siluro-Devonian clastic and carbonate rocks, yielded a single-polarity component that clusters better before any correction,

with declinations consistently to the south and equatorial paleolatitudes (Figure 4 and Table 1). This indicates that the magnetization must have been acquired when Iberia was situated at equatorial latitudes during a long-lasting reverse chron, since no polarity changes have been found. We know that Iberia crossed the equator line from the Southern to Northern Hemisphere during the Early Permian (Osete et al., 1997; Weil et al., 2010) and migrated, together with Pangea, rapidly toward the north (Torsvik et al., 2012). We suggest that rocks acquired component P at Early Permian at Early Permian times during the Permo-Carboniferous reversed superchron (PCRS) ranging ~314–265 Ma (Langereis et al., 2010). Therefore, this magnetization is likely primary for the Early Permian mafic dykes and sills that intruded and subsequently overprinted the Devonian sedimentary sequence. There is a small but significant difference in inclination between the remagnetized vector in the sedimentary rocks (4.5° ± 4.7°) and the potentially primary magnetization found in the delerite dykes/sills (−8.8° ± 6.9°). This divergence may indicate that rocks were magnetized at slightly different times, with the overprint being an earlier magnetization, perhaps fluid driven, when Iberia was still in the Southern Hemisphere. Also, the magnetization in the Early Permian mafic dykes and sills shows a noncircular VGP, in contrast to the remagnetized Devonian clastic and carbonates. We interpret the elongated shape as a not fully averaged paleosecular variation of the geomagnetic field, likely due to undersampling those Early Permian dolerites. Calvin et al. (2014) described a very similar component in Early Permian intrusions in an equivalent area of the Iberian Range.

Component P shows inclinations very similar to Component eP for stable Iberia of Weil et al. (2010), but it is rotated ~22° CW with respect to eP. This rotation coincides with the rotation recorded by the Cenozoic and Mesozoic clastic and carbonatic rocks of the Aragonese Branch of the Iberian Range (21° CW following H. J. Mauritsch et al., personal communication, 2018) during the Alpine orogeny. We conclude that the only post-Permian event that the studied Paleozoic rocks recorded is a ~22° CW vertical axis rigid-body rotation together with Mesozoic and Cenozoic rocks possibly related to Alpine basement thrusting that underwent differential displacement along strike during its movement (E. Izquierdo-Llavall et al., personal communication, 2018).

4.1.2. Component #1

Component #1 is a single-polarity reverse component that does not pass a fold test (Figure 5). It represents a shallow component from the Southern Hemisphere (Dec./Inc. = 150.4°/8.3°; Table 1). The magnetization of this component must therefore have been acquired before Iberia crossed the equator in the Early Permian (Weil et al., 2010) but after the onset of the PCRS (~314 Ma), constraining Component #1 to be a late Carboniferous overprint. If we correct for the ~22° CW Cenozoic rotation, this component shows a ~25° counterclockwise (CCW) rotation with respect to the Early Permian pole for stable Iberia (Weil et al., 2010). A CCW rotation during the latest Carboniferous is consistent with the Cantabrian Orocline sense and timing of rotation (e.g., Weil et al., 2013). Considering the strike of the Iberian range, however, the expected magnitude of rotation would be higher. For this reason, we consider Component #1 to be a late Carboniferous overprint that occurred at the latest stages of Cantabrian Orocline formation.

4.1.3. Component #2

We identified Component #2 in 46 specimens from different sites within the Santa Cruz syncline (Data Set S2). Component #2 passes the fold test and shows both normal and reverse polarity distributions that pass a reversal test (Figure 6). The two positive field tests would support a (pseudo) primary magnetization (e.g., van der Voo, 1990). However, the scarce available paleomagnetic data for Siluro-Devonian times indicate that the northern margin of Gondwana and the derived terranes (e.g., Armorica) were at latitudes of 30–40°S (Hansma et al., 2015; Torsvik et al., 2012). More importantly, biostratigraphic and faunal constraints from the Santa Cruz syncline support a medium-latitude (~23° to ~66°) formation for the sampled units (Carls, 1988; Villas, 1995). Therefore, the inclinations found (12.7° ± 11.7°) are too shallow when compared to the geological constraints, indicating a magnetization acquired when the rocks were at nearly equatorial paleolatitudes (λ = 6.4° S ± ~6°). Following the global apparent polar wander path of Torsvik et al. (2012) calculated for Iberia (given in Koymans et al., 2016) such low paleolatitude (6.4°S) would only be expected for Iberia in middle–late Carboniferous times, during the waning stages of the Variscan orogeny. The Variscan orogeny produced pervasive remagnetizations in Iberia (e.g., Pastor-Galán, Gutiérrez-Alonso, et al., 2017; Pastor-Galán, Mulchrone, et al., 2017; Weil et al., 2013). Therefore, we suggest a Late Mississippian–Early Pennsylvanian (middle Carboniferous) secondary origin for Component #2. The remagnetization likely occurred just before the onset of the long-lasting PCRS (ca. 314 Ma), allowing the occurrence of two polarities.
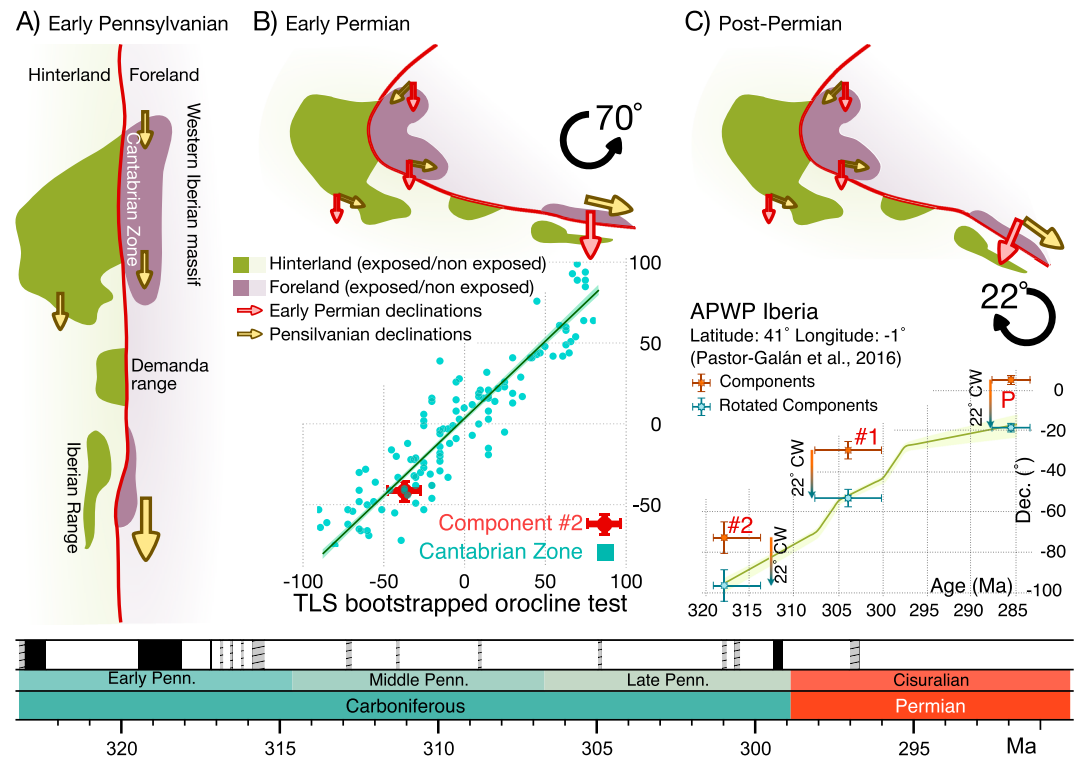
Figure 7. Cartoon depicting the different vertical axis rotation events that occurred in the Iberian Range. (a) Original quasi-linear Variscan Belt. (b) The formation of the Cantabrian Orocline at the Carboniferous–Permian boundary involved a ~70° counterclockwise rotation in the area, which fully corresponds with the expected rotation, considering the strike of the Variscan structures in the Iberian Range as shown by the perfect fit of Component #2 in the orocline test for the Cantabrian Zone (below). (c) Cenozoic rotation of ~22° clockwise (CW) likely produced by differential shortening during the Alpine orogeny (E. Izquierdo-Llavall et al., personal communication, 2018). Note that once this 22° CW rotation is corrected, Components #2, #1, and P fit perfectly with the apparent polar wander path (APWP) for the southern limb of the orocline (Pastor-Galán et al., 2016). Below, the global magnetic polarity time scale for the Pennsylvanian and Cisuralian (following Ogg et al., 2016). TLS = Total Least Squares.

4.2. On the Central Iberian Curve and Extent of the Cantabrian Orocline

Our new paleomagnetic results show a vertical axis rotation of ~22° CW of the Early Permian Component P (Figure 7) with respect to stable Iberia at that time (Weil et al., 2010). This 22° rotation is identical to the rotation observed in overlying Mesozoic and Early Cenozoic rocks in the area (H. J. Mauritsch et al., personal communication, 2018). Our results also establish a differential pre-Permian CCW rotation recorded by Components #1 (~25°) and #2 (~80°) with respect to Component P. Component #1 shows a CCW rotation of less magnitude (~25°) and, like P, only reverse polarity. We interpret Component #1 as an overprint occurring during the Cantabrian Orocline formation, sometime between ~310 and 295 Ma (Pastor-Galán, Groenewegen, et al., 2015; Pastor-Galán, Gutiérrez-Alonso, et al., 2017; Pastor-Galán, Mulchrone, et al., 2017). This interpretation explains the similar inclination, declination, and single polarity (Figure 7). The change in structural trend in the Paleozoic rocks of the Iberian Range corresponds roughly to 25° (Figure 7). We have calculated a rotation of 22° around an Euler pole located where the strike of the orogen changes in the Iberian Range (42°N, 2.4 W), and the results coincide with the Iberian apparent polar wander path for the late Carboniferous (Pastor-Galán et al., 2016) (Figure 7). After the 22° CW Cenozoic rotation was restored, the structural trend of the Paleozoic outcrops of the Aragonese Branch of the Iberian Range become near parallel to the orogen strike in the southern limb of the Cantabrian Orocline (Figures 1 and 7). When accounting for the 22° CW, Component #2 shares a common distribution (following the coordinate bootstrap test of Tauxe, 2010) with the Late Mississippian–Early Pennsylvanian pole of Iberia calculated by Pastor-Galán et al. (2016; Figure S3).

Once the structure and the paleomagnetic results are restored to a pre-Alpine rotation, Component #2 can be compared with the orocline test of the Cantabrian Zone. We have plotted Component #2 into the
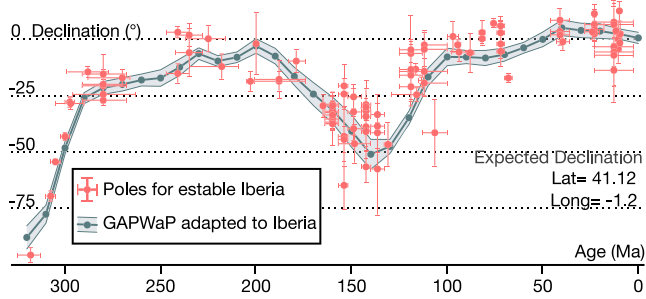
Figure 8. Global apparent polar wander path (GAPWaP; Torsvik et al., 2012) adapted to the Euler pole rotations chosen to reconstruct Iberia and a paleomagnetic compilation of Iberian poles from Dinarès-Turell et al. (2005), Vissers et al. (2016), Pastor-Galán et al. (2016), Pastor-Galán, Gutiérrez-Alonso, et al. (2017), and Pastor-Galán, Mulchrone, et al. (2017).

bootstrapped orocline test for the Cantabrian Orocline (Pastor-Galán, Gutiérrez-Alonso, et al., 2017; Pastor-Galán, Mulchrone, et al., 2017) obtaining a perfect fit (Figure 7c). Thus, Component #2 shows the paleolatitude and CCW rotation at ~320 Ma (Figures 7 and 8) expected at the southern limb of the Cantabrian Orocline. Our data indicate that most of the Iberia rotated ~70° CCW with the exception of the very north (at present-day coordinates) where the hinge of the Cantabrian Orocline is located, and including the Pyrenees (Figure 1). Therefore, the extent of the vertical axis rotations associated with the Cantabrian Orocline formation is much larger than originally hypothesized.

Our results show that the change in trend in the Aragonese Branch of the Iberian Range has a Cenozoic (Alpine) rather than a Paleozoic (Variscan) origin. The new data presented in this paper not only confirm the nonsecondary nature of the Central Iberian curve claimed by Pastor-Galán, Groenewegen, et al. (2015), Pastor-Galán et al. (2016), Pastor-Galán, Gutiérrez-Alonso, et al. (2017), and Pastor-Galán, Mulchrone, et al. (2017), but rules out the idea of a single tectonic process responsible for the observed curvature. We claim that the geometry of the Central Iberian curve is the results of a combination of processes. The curvature of the inner arc (Galicia-Trás-os-Montes; Figure 1), if rotational, has to be the result of a process before ~318 Ma, probably during the early stages of collision and involving no vertical axis rotations (Pastor-Galán, Dias da Silva, et al., 2018; Jacques, Muchez, et al., 2018; Jacques, Vieira, et al., 2018). The outer arc curvature, at least in the Iberian Range, is the result of much younger Alpine tectonics: These are commonly disregarded in studies of the Variscan orogen of Iberia.

We have also produced an Iberian plate (including all Iberia located to the south of the hinge of the Cantabrian Orocline) version of the global apparent polar wander path (Torsvik et al., 2012) accounting for the rotation of the Cantabrian Orocline. For this, we used the databases from Dinarès-Turell et al. (2005) and Vissers et al. (2016; Figure 8 and Table 2) and all data from the southern limb of the Cantabrian Orocline (Pastor-Galán et al., 2016; Pastor-Galán, Gutiérrez-Alonso, et al., 2017; Pastor-Galán, Mulchrone, et al., 2017; this study). Figure 8 and Table 2 show the best fit Euler poles to apply to the global apparent polar wander path. To fulfill all these paleomagnetic constraints, a large amount of convergence and/or extension must have been accommodated somewhere in the core of Pangea. These convergence and extension would require the development of large basins and/or at least one subduction zone (either oceanic or intracontinental). Although those features are yet to be described, the Iberia was extensively intruded by mantle-derived rocks during that particular time interval (e.g., Gutiérrez-Alonso, Fernández-Suárez, et al., 2011; Pereira et al., 2014). The mantle character of the intrusions (Perini et al., 2004; Gutiérrez-Alonso, Murphy, et al., 2011) points toward some sort of lithospheric foundering (e.g., subduction slab break-off and delamination). In addition, Pereira et al. (2014, 2015) speculated with subduction of the Paleotethys below eastern Iberia as the trigger for late Carboniferous–Early Permian magmatism.

There is an ongoing debate on how and when Pangea became a rigid supercontinent (e.g., Gallo et al., 2017) with contrasting age estimations ranging between ca. 330 to 240 Ma (e.g., Blakey and Ranney, 2017; Veevers, 2004). The results showed in this paper, together with those from the Munster basin in Ireland (Pastor-Galán, Ursem, et al., 2015), show the Cantabrian Orocline as a continental scale feature that affected all levels of the lithosphere (Weil et al., 2013). We think that the evidence is enough to state that Pangea did not behave as a rigid superplate at least until ca. 295 Ma.

Table 2
Euler Poles to Adapt GAPWaP for Africa (Torsvik et al., 2012) to the Iberian Plate as Shown in Figure 8

Age	Lat	Lon	Rot
0	0	0	0
10	14.67	−19.18	1.01
20	15.32	−19.19	2.39
30	22.3	−19.38	3.31
40	30.76	−15.43	6.16
50	30.2	−17.97	6.63
60	31.83	−18.34	7.02
70	29.96	−18.88	7.05
80	31.4	−18.59	8.04
90	36.64	−15.28	11.35
100	40.47	−12.35	15.93
110	42.64	−10.4	20.57
120	40.17	−13.9	7.25
130	62.66	−20.3	−2.86
140	61.86	−31.28	−2.7
150	73.26	−101.4	−1.27
160	21.37	0.47	5.94
170	52.67	−4.17	13.89
180	49.61	−3.41	17.46
190	47.75	−3.19	21.11
200	46.52	2.52	19.18
210	54.3062	19.8089	17.4185
230	50.1173	5.6959	23.1255
290	51.711	8.43871	18.4491
300	6.3921	−36.697	−6.09675
310	36.7237	−10.4128	−34.9562
320	38.0322	−9.26327	−48.0554

Note. GAPWaP = global apparent polar wander path.

5. Conclusions

Our paleomagnetic and structural results from the Santa Cruz syncline (Aragonese Branch of the Iberian Range) show a vertical axis rotation of ~22° CW during the Cenozoic and about 70° CCW during the late Carboniferous. Once the Cenozoic rotation is accounted for, the structural and paleomagnetic trends of the Aragonese Branch become parallel to those in the southern limb of the Cantabrian Orocline, ruling out a Variscan origin for the outer Central Iberian curve. Thus, the Central Iberian curve is a structure resulted from a combination of processes: (1) an Early Variscan nonrotational process in its core and (2) a Cenozoic CW rotation in its outer arc. In addition, the fit of the Aragonese Branch of the Iberian Range with the Cantabrian Zone indicates that most of the Iberia rotated at least 70° CCW with the exception of its hinge (located at the northwest of the Iberian Peninsula). This means that the extent of the vertical axis rotations associated to the Cantabrian Orocline formation is much larger than previously thought. Using the most recent paleomagnetic constraints and GPlates (Boyden et al., 2011), we have quantified in 1,000 km the minimum amount of convergence in the core of Pangea required to accommodate the rotations in Iberia associated with the Cantabrian Orocline.

References

Aerden, D. (2004). Correlating deformation in Variscan NW-Iberia using porphyroblasts; implications for the Ibero-Armorican Arc. *Journal of Structural Geology*, *26*(1), 177–196. https://doi.org/10.1016/S0191-8141(03)00070-1

Alvaro, M., Capote, R., & Vegas, R. (1978). Un modelo de evolución geotectónica para la Cadena Celtibérica. *Acta Geologica Hispánica*, *14*, 172–177.

Ballèvre, M., Martinez Catalan, J. R., Lopez-Carmona, A., Pitra, P., Abati, J., Fernandez, R. D., et al. (2014). Correlation of the nappe stack in the Ibero-Armorican Arc across the Bay of Biscay: A joint French-Spanish project. *Geological Society, London, Special Publications*, *405*(1), 77–113. https://doi.org/10.1144/SP405.13

Barreiro, J. G., Wijbrans, J. R., Castineiras, P., Catalan, J. R. M., Arenas, R., Garcia, F. D., & et al. (2006). Ar-40/Ar-39 laserprobe dating of mylonitic fabrics in a polyorogenic terrane of NW Iberia. *Journal of the Geological Society*, *163*(1), 61–73. https://doi.org/10.1144/0016-764905-012

Belica, M. E., Tohver, E., Pisarevsky, S. A., Jourdan, F., Denyszyn, S., & George, A. D. (2017). Middle Permian paleomagnetism of the Sydney Basin, Eastern Gondwana: Testing Pangea models and the timing of the end of the Kiaman Reverse Superchron. *Tectonophysics*, *699*, 178–198. https://doi.org/10.1016/J.TECTO.2016.12.029

Blakey, R. C., & Ranney, W. D. (2017). Ancient Landscapes of Western North America: A Geologic History with Paleogeographic Maps. Springer.

Blakey, R. C., & Ranney, W. D. (2018). The amalgamation of Pangaea and the Sonoma orogeny: Early Permian to Early Triassic—Ca. 300–240 Ma. In *Ancient landscapes of western North America* (pp. 83–88). Cham: Springer International Publishing. https://doi.org/10.1007/978-3-319-59636-5_6

Borradaile, G. J. (1988). Magnetic susceptibility, petrofabrics and strain. *Tectonophysics*, *156*(1-2), 1–2), 1–20. https://doi.org/10.1016/0040-1951(88)90279-X

Boyden, J. A., Müller, R. D., Gurnis, M., Torsvik, T. H., Clark, J. A., Turner, M., et al. (2011). Next-generation plate-tectonic reconstructions using GPlates. In G. R. Keller, & C. Baru (Eds.), *Geoinformatics: Cyberinfrastructure for the solid earth sciences* (pp. 95–113). Cambridge, UK: Cambridge University Press. https://doi.org/10.1017/CBO9780511976308.008

Bozkurt, E., Francisco Pereira, M., Strachan, R., & Quesada, C. (2008). Evolution of the Rheic Ocean. *Tectonophysics*, *461*(1–4), 1–8.

Butler, R. F. (1992). *Paleomagnetism: magnetic domains to geologic terranes* (Vol. 319). Boston: Blackwell Scientific Publications.

Calvin, P., Casas, A. M., Villalaín, J. J., & Tierz, P. (2014). Reverse magnetic anomaly controlled by Permian igneous rocks in the Iberian Chain (N Spain). *Geologica Acta*, *12*(3), 193–207. https://doi.org/10.1344/GeologicaActa2014.12.3.2

Calvín-Ballester, P., & Casas-Sainz, A. M. (2014). Folded Variscan thrust in the Herrera unit of the Iberian Range (NE Spain). In F. Bastida, S. Llana-Fúnez, & A. Marcos (Eds.), *Deformation structures and processes within the continental crust*, *Special Publications* (Vol. 394, pp. 39–52). London: Geological Society.

Carls, P. (1983). La Zona Asturoccidental-Leonesa en Aragón y el Macizo del Ebro como prolongación del Macizo Cantábrico. In *Libro Jubilar J. M. Ríos, Geologia de España*, (Vol. 3, pp. 11–32). Madrid: Instituto Geológico y Minero de España.

Carls, P. (1988). The Devonian of Celtiberia (Spain) and Devonian paleogeography of SW Europe. In N. J. McMillan, A. F. Embry, & D. J. Class (Eds.), *Devonian of the world*, *Canadian Society of Petroleum Geologist, Memoir* (Vol. 14, pp. 421–466). Calgary, Alberta.

Casas-Sainz, A. M., & Faccenna, C. (2001). Tertiary compressional deformation of the Iberian plate. *Terra Nova*, *13*(4), 281–288. https://doi.org/10.1046/j.1365-3121.2001.00355.x

Cifelli, F., Mattei, M., Chadima, M., Hirt, A. M., & Hansen, A. (2005). The origin of tectonic lineation in extensional basins: Combined neutron texture and magnetic analyses on 'undeformed' clays. *Earth and Planetary Science Letters*, *235*(1-2), 62–78. https://doi.org/10.1016/j.epsl.2005.02.042

Cortes Gracia, A. L., & Casas-Sáinz, A. M. (1996). Deformación alpina de zócalo y cobertera en el borde norte de la Cordillera Ibèrica (Cubeta de Azuara-Sierra de Herrera). *Revista de la Sociedad Geológica de España*, *9*(1), 51–66.

Dallmeyer, R. D., Catalán, J. R. M., Arenas, R., Gil Ibarguchi, J. I., Gutiérrez^Alonso, G., Farias, P., et al. (1997). Diachronous Variscan tecto-nothermal activity in the NW Iberian massif: Evidence from $^{40}Ar/^{39}Ar$ dating of regional fabrics. *Tectonophysics*, *277*(4), 307–337. https://doi.org/10.1016/S0040-1951(97)00035-8

Deenen, M. H. L., Langereis, C. G., van Hinsbergen, D. J. J., & Biggin, A. J. (2011). Geomagnetic secular variation and the statistics of palaeomagnetic directions. *Geophysical Journal International*, *186*, 509–520.

de Vicente, G., Vegas, R., Muñoz-Martín, A., van Wees, J. D., Casas-Sáinz, A. M., Sopeña, A., & et al. (2009). Oblique strain partitioning and transpression on an inverted rift: The Castilian Branch of the Iberian Chain. *Tectonophysics*, *470*(3-4), 224–242. https://doi.org/10.1016/j.tecto.2008.11.003

Dinarès-Turell, J., Diez, J. B., Rey, D., & Arnal, I. (2005). "Buntsandstein" magnetostratigraphy and biostratigraphic reappraisal from eastern Iberia: Early and Middle Triassic stage boundary definitions through correlation to Tethyan sections. *Palaeogeography, Palaeoclimatology, Palaeoecology*, *229*(1–2), 158–177. https://doi.org/10.1016/J.PALAEO.2005.06.036

Domeier, M. (2016). A plate tectonic scenario for the Iapetus and Rheic Oceans. *Gondwana Research*, *36*, 275–295. https://doi.org/10.1016/j.gr.2015.08.003

Domeier, M., & Torsvik, T. H. (2014). Plate tectonics in the late Paleozoic. *Geoscience Frontiers*, *5*(3), 303–350.

Domeier, M., van der Voo, R., & Torsvik, T. H. (2012). Paleomagnetism and Pangea: The road to reconciliation. *Tectonophysics*, *514-517*, 14–43. https://doi.org/10.1016/j.tecto.2011.10.021

Fisher, R. (1953). Dispersion on a sphere. *Proceedings of the Royal Society A: Mathematical, Physical and Engineering Sciences*, *217*(1130), 295–305. https://doi.org/10.1098/rspa.1953.0064

Gallo, L. C., Tomezzoli, R. N., & Cristallini, E. O. (2017). A pure dipole analysis of the Gondwana apparent polar wander path: Paleogeographic implications in the evolution of Pangea. *Geochemistry, Geophysics, Geosystems*, *18*, 1499–1519. https://doi.org/10.1002/2016GC006692

García-Lasanta, C., Casas Sainz, A., Villalaín, J. J., Oliva-Urcia, B., Speranza, F., & Mochales, T. (2017). Remagnetizations used to unravel large-scale fold kinematics: A case study in the Cameros basin (N Spain). *Tectonics*, *36*, 714–729. https://doi.org/10.1002/2016TC004459

García-Lasanta, C., Oliva-Urcia, B., Román-Berdiel, T., Casas, A. M., Gil-Peña, I., Sánchez-Moya, Y., et al. (2015). Evidence for the Permo-Triassic transtensional rifting in the Iberian Range (NE Spain) according to magnetic fabrics results. *Tectonophysics*, *651-652*, 216–231. https://doi.org/10.1016/j.tecto.2015.03.023

García-López, S., Bastida, F., Aller, J., Sanz-López, J., Marín, J. A., & Blanco-Ferrera, S. (2013). Tectonothermal evolution of a major thrust system: The Esla-Valsurbio unit (Cantabrian Zone, NW Spain). *Geological Magazine*, *150*(6), 1047–1061. https://doi.org/10.1017/S0016756813000071

Gong, Z., Langereis, C. G., & Mullender, T. A. T. (2008). The rotation of Iberia during the Aptian and the opening of the Bay of Biscay. *Earth and Planetary Science Letters*, *273*(1–2), 80–93.

Gozalo, R., & Liñan, E. (1988). Los materiales hercínicos de la Cordillera Ibérica en el contexto del Macizo Ibérico. *Estudios Geológicos*, *44*(5–6), 399–404.

Guimerà, J., Mas, R., & Alonso, Á. (2004). Intraplate deformation in the NW Iberian Chain: Mesozoic extension and Tertiary contractional inversion. *Journal of the Geological Society*, *161*(2), 291–303. https://doi.org/10.1144/0016-764903-055

Gutiérrez-Alonso, G., Fernández-Suárez, J., Jeffries, T. E., Johnston, S. T., Pastor-Galán, D., Murphy, J. B., et al. (2011). Diachronous post-orogenic magmatism within a developing orocline in Iberia, European Variscides. *Tectonics*, *30*, TC5008. https://doi.org/10.1029/2010TC002845

Gutiérrez-Alonso, G., Johnston, S. T., Weil, A. B., Pastor-Galán, D., & Fernández-Suárez, J. (2012). Buckling an orogen: The Cantabrian Orocline. *GSA Today*, *22*(7), 4–9.

Gutiérrez-Alonso, G., Murphy, J. B., Fernández-Suárez, J., Weil, A. B., Franco, M. P., & Gonzalo, J. C. (2011). Lithospheric delamination in the core of Pangea: Sm-Nd insights from the Iberian mantle. *Geology*, *39*(2), 155–158. https://doi.org/10.1130/G31468.1

Hansma, J., Tohver, E., Yan, M., Trinajstic, K., Roelofs, B., Peek, S., et al. (2015). Late Devonian carbonate magnetostratigraphy from the Oscar and Horse Spring Ranges, Lennard Shelf, Canning Basin, Western Australia. *Earth and Planetary Science Letters*, *409*, 232–242. https://doi.org/10.1016/j.epsl.2014.10.054

Jacques, D., Muchez, P., & Sintubin, M. (2018). Superimposed folding and W-Sn vein-type mineralisation in the Central Iberian Zone associated with late-Variscan oroclinal buckling: A structural analysis from the Regoufe area (Portugal). *Tectonophysics*, *742*, 66–83.

Jacques, D., Vieira, R., Muchez, P., & Sintubin, M. (2018). Transpressional folding and associated cross-fold jointing controlling the geometry of post-orogenic vein-type W-Sn mineralization: Examples from Minas da Panasqueira, Portugal. *Mineralium Deposita*, *53*(2), 171–194. https://doi.org/10.1007/s00126-017-0728-6

Johnston, S. T., Weil, A. B., & Gutiérrez-Alonso, G. (2013). Oroclines: Thick and thin. *GSA Bulletin*, *125*(5-6), 643–663. https://doi.org/10.1130/B30765.1

Juárez, M. ., Lowrie, W., Osete, M. ., & Meléndez, G. (1998). Evidence of widespread Cretaceous remagnetisation in the Iberian Range and its relation with the rotation of Iberia. *Earth and Planetary Science Letters*, *160*(3–4), 729–743. https://doi.org/10.1016/S0012-821X(98)00124-1

Juárez, M. T., Osete, M. L., Meléndez, G., Langereis, C. G., & Zijderveld, J. D. A. (1994). Oxfordian magnetostratigraphy of the Aguilón and Tosos sections (Iberian Range, Spain) and evidence of a pre-Oligocene overprint. *Physics of the Earth and Planetary Interiors*, *85*(1–2), 195–211. https://doi.org/10.1016/0031-9201(94)90017-5

Kirschvink, J. L. (1980). The least-squares line and plane and the analysis of palaeomagnetic data. *Geophysical Journal International*, *62*(3), 699–718. https://doi.org/10.1111/j.1365-246X.1980.tb02601.x

Kollmeier, J. M., van der Pluijm, B. A., & van der Voo, R. (2000). Analysis of Variscan dynamics; early bending of the Cantabria-Asturias arc, northern Spain. *Earth and Planetary Science Letters*, *181*(1–2), 203–216. https://doi.org/10.1016/S0012-821X(00)00203-X

Koymans, M. R., Langereis, C. G., Pastor-Galán, D., & van Hinsbergen, D. J. J. (2016). Paleomagnetism.org: An online multi-platform open source environment for paleomagnetic data analysis. *Computers and Geosciences*, *93*, 127–137. https://doi.org/10.1016/j.cageo.2016.05.007

Langereis, C. G., Krijgsman, W., Muttoni, G., & Menning, M. (2010). Magnetostratigraphy—Concepts, definitions, and applications. *Newsletters on Stratigraphy*, *43*(3), 207–233. https://doi.org/10.1127/0078-0421/2010/0043-0207

López-Carmona, A., Abati, J., Pitra, P., & Lee, J. K. W. (2014). Retrogressed lawsonite blueschists from the NW Iberian massif: P–T–t constraints from thermodynamic modelling and ^{40}Ar/^{39}Ar geochronology. *Contributions to Mineralogy and Petrology*, *167*(3), 987. https://doi.org/10.1007/s00410-014-0987-5

Martínez Catalán, J. R. (2011). Are the oroclines of the Variscan belt related to late Variscan strike-slip tectonics? *Terra Nova*, *23*(4), 241–247.

Mac Niocaill, C. (2000). A new Silurian palaeolatitude for eastern Avalonia and evidence for crustal rotations in the Avalonian margin of southwestern Ireland. *Geophysical Journal International*, *141*(3), 661–671. https://doi.org/10.1046/j.1365-246x.2000.00101.x

Martínez Catalán, J. R. (2012). The Central Iberian arc, an orocline centered in the Iberian massif and some implications for the Variscan Belt. *International Journal of Earth Sciences*, *101*(5), 1299–1314. https://doi.org/10.1007/s00531-011-0715-6

Martínez Catalán, J. R., Aerden, D. G. A. M., & Carreras, J. (2015). The "Castilian bend" of Rudolf Staub (1926): Historical perspective of a forgotten orocline in Central Iberia. *Swiss Journal of Geosciences*, *108*(2–3), 289–303. https://doi.org/10.1007/s00015-015-0202-3

Mattei, M., Sagnotti, L., Faccenna, C., & Funiciello, R. (1997). Magnetic fabric of weakly deformed clay-rich sediments in the Italian peninsula: Relationship with compressional and extensional tectonics. *Tectonophysics*, *271*(1-2), 107–122. https://doi.org/10.1016/S0040-1951(96)00244-2

McFadden, P. L., & McElhinny, M. W. (1988). The combined analysis of remagnetization circles and direct observations in palaeomagnetism. *Earth and Planetary Science Letters*, *87*(1–2), 161–172. https://doi.org/10.1016/0012-821X(88)90072-6

Nance, R. D., Gutiérrez-Alonso, G., Keppie, J. D., Linnemann, U., Murphy, J. B., Quesada, C., et al. (2010). Evolution of the Rheic Ocean. *Gondwana Research*, *17*(2–3), 194–222. https://doi.org/10.1016/j.gr.2009.08.001

Ogg, J. G., Ogg, G., & Gradstein, F. M. (2016). A concise geologic time scale: 2016. Elsevier.

Oliva-Urcia, B., Larrasoaña, J. C., Pueyo, E. L., Gil, A., Mata, P., Parés, J. M., et al. (2009). Disentangling magnetic subfabrics and their link to deformation processes in cleaved sedimentary rocks from the Internal Sierras (west central Pyrenees, Spain). *Journal of Structural Geology*, *31*(2), 163–176.

Osete, M. L., Rey, D., Villalaín, J. J., & Juárez, M. T. (1997). The Late Carboniferous to Late Triassic segment of the apparent polar wander path of Iberia. *Geologie en Mijnbouw*, *76*(1–2), 105–119.

Pares, J. M. (2015). Sixty years of anisotropy of magnetic susceptibility in deformed sedimentary rocks. *Frontiers in Earth Science*, *3*, 1–13. https://doi.org/10.3389/feart.2015.00004

Pastor-Galán, D., Dekkers, M. J., Gutiérrez-Alonso, G., Brouwer, D., Groenewegen, T., Krijgsman, W., et al. (2016). Paleomagnetism of the Central Iberian curve's putative hinge: Too many oroclines in the Iberian Variscides. *Gondwana Research*, *39*, 96–113. https://doi.org/10.1016/j.gr.2016.06.016

Pastor-Galán, D., Dias da Silva, I. F., Groenewegen, T., & Krijgsman, W. (2018). Tangled up in folds: Tectonic significance of superimposed folding at the core of the Central Iberian curve (West Iberia). *International Geology Review*, 1–16. https://doi.org/10.1080/00206814.2017.1422443

Pastor-Galán, D., Groenewegen, T., Brouwer, D., Krijgsman, W., & Dekkers, M. J. (2015). One or two oroclines in the Variscan orogen of Iberia? Implications for Pangea amalgamation. *Geology*, *43*(6), 527–530. https://doi.org/10.1130/G36701.1

Pastor-Galán, D., Gutiérrez-Alonso, G., Dekkers, M. J., & Langereis, C. G. (2017). Paleomagnetism in Extremadura (Central Iberian Zone, Spain) Paleozoic rocks: Extensive remagnetizations and further constraints on the extent of the Cantabrian orocline. *Journal of Iberian Geology*, *43*(4), 583–600. https://doi.org/10.1007/s41513-017-0039-x

Pastor-Galán, D., Gutiérrez-Alonso, G., Fernández-Suárez, J., Murphy, J. B., & Nieto, F. (2013). Tectonic evolution of NW Iberia during the Paleozoic inferred from the geochemical record of detrital rocks in the Cantabrian Zone. *Lithos*, *182-183*, 211–228. https://doi.org/10.1016/j.lithos.2013.09.007

Pastor-Galán, D., Gutiérrez-Alonso, G., Meere, P. A., & Mulchrone, K. F. (2009). Factors affecting finite strain estimation in low-grade, low-strain clastic rocks. *Journal of Structural Geology*, *31*(12), 1586–1596. https://doi.org/10.1016/j.jsg.2009.08.005

Pastor-Galán, D., Gutiérrez-Alonso, G., Mulchrone, K. F., & Huerta, P. (2012). Conical folding in the core of an orocline. A geometric analysis from the Cantabrian Arc (Variscan Belt of NW Iberia). *Journal of Structural Geology*, *39*, 210–223. https://doi.org/10.1016/j.jsg.2012.02.010

Pastor-Galán, D., Gutiérrez-Alonso, G., & Weil, A. B. (2011). Orocline timing through joint analysis: Insights from the Ibero-Armorican Arc. *Tectonophysics*, *507*(1–4), 31–46. https://doi.org/10.1016/j.tecto.2011.05.005

Pastor-Galan, D., Gutierrez-Alonso, G., Zulauf, G., & Zanella, F. (2012). Analogue modeling of lithospheric-scale orocline buckling: Constraints on the evolution of the Iberian-Armorican Arc. *Geological Society of America Bulletin*, *124*(7–8), 1293–1309. https://doi.org/10.1130/B30640.1

Pastor-Galán, D., Mulchrone, K. F., Koymans, M. R., van Hinsbergen, D. J. J., & Langereis, C. G. (2017). Bootstrapped total least squares orocline test: A robust method to quantify vertical-axis rotation patterns in orogens, with examples from the Cantabrian and Aegean oroclines. *Lithosphere*, *9*(3), 499–511. https://doi.org/10.1130/L547.1

Pastor-Galán, D., Nance, R. D., Murphy, J. B., & Spencer, C. J. (2018). Supercontinents: Myths, mysteries, and milestones. *Geological Society, London, Special Publications*, *470*, SP470–SP416.

Pastor-Galán, D., Ursem, B., Meere, P. A., & Langereis, C. (2015). Extending the Cantabrian Orocline to two continents (from Gondwana to Laurussia). Paleomagnetism from South Ireland. *Earth and Planetary Science Letters*, *432*, 223–231. https://doi.org/10.1016/j.epsl.2015.10.019

Pereira, M. F., Castro, A., Chichorro, M., Fernández, C., Díaz-Alvarado, J., Martí, J., & et al. (2014). Chronological link between deep-seated processes in magma chambers and eruptions: Permo-Carboniferous magmatism in the core of Pangaea (Southern Pyrenees). *Gondwana Research*, *25*(1), 290–308. https://doi.org/10.1016/j.gr.2013.03.009

Pereira, M. F., Castro, A., & Fernandez, C. (2015). The inception of a Paleotethyan magmatic arc in Iberia. *Geoscience Frontiers*, *6*(2), 297–306. https://doi.org/10.1016/j.gsf.2014.02.006

Pereira, M. F., Gama, C., & Rodríguez, C. (2017). Coeval interaction between magmas of contrasting composition (late Carboniferous–Early Permian Santa Eulália-Monforte massif, Ossa-Morena Zone): Field relationships and geochronological constraints. *Geologica Acta*, *15*(4), 409–428.

Pereira, M. F., Gutíerrez-Alonso, G., Murphy, J. B., Drost, K., Gama, C., & Silva, J. B. (2017). Birth and demise of the Rheic Ocean magmatic arc(s): Combined U–Pb and Hf isotope analyses in detrital zircon from SW Iberia siliciclastic strata. *Lithos*, *278*, 383–399.

Pérez-Cáceres, I., Martínez Poyatos, D., Simancas, J. F., & Azor, A. (2015). The elusive nature of the Rheic Ocean suture in SW Iberia. *Tectonics*, *34*, 2429–2450. https://doi.org/10.1002/2015TC003947

Pérez-Estaún, A., Martínez-Catalán, J. R., & Bastida, F. (1991). Crustal thickening and deformation sequence in the footwall to the suture of the Variscan belt of northwest Spain. *Tectonophysics*, *191*(3–4), 243–253.

Pérez-Estaún, A., Bastida, F., Martínez Catalán, J. R., Gutiérrez-Marco, J. C., Marcos, A., & Pulgar, J. A. (1990). West Asturian-Leonese Zone. Stratigraphy. In *Pre-Mesozoic Geology of Iberia* (pp. 92–102). Berlin: Springer.

Pérez-Pueyo, M., Bádenas, B., & Villas, E. (2018). Sedimentology and paleontology of the lower member of the Nogueras Fm (Lower Devonian) at Santa Cruz de Nogueras (Teruel, NE Spain). *Revista de la Sociedad Geológica de España*, *31*(1).

Perini, G., Cebria, J. M., Lopez-Ruiz, J., & Doblas, M. (2004). Carboniferous–Permian mafic magmatism in the Variscan belt of Spain and France: Implications for mantle sources. *Geological Society, London, Special Publications*, *223*(1), 415–438.

Pueyo, E. L., Oliva-Urcia, B., Sussman, A. J., & Cifelli, F. (2016). Palaeomagnetism in fold and thrust belts: Use with caution. In E. L. Pueyo, F. Cifelli, A. Sussman, & B. Oliva-Urcia (Eds.), *Palaeomagnetism in fold and thrust belts: New perspectives*, *Special Publication*, (Vol. 425, pp. 259–276). London: Geological Society. https://doi.org/10.1144/SP425.14

Ramón, M. J., Pueyo, E. L., Oliva-Urcia, B., & Larrasoaña, J. C. (2017). Virtual directions in paleomagnetism: A global and rapid approach to evaluate the NRM components. *Frontiers in Earth Science*, *5*, 8.

Roca, E., & Guimerà, J. (1992). The Neogene structure of the eastern Iberian margin: Structural constraints on the crustal evolution of the Valencia trough (western Mediterranean). *Tectonophysics*, *203*(1-4), 203–218. https://doi.org/10.1016/0040-1951(92)90224-T

Salas, R., & Casas, A. (1993). Mesozoic extensional tectonics, stratigraphy and crustal evolution during the Alpine cycle of the eastern Iberian basin. *Tectonophysics*, *228*(1-2), 33–55. https://doi.org/10.1016/0040-1951(93)90213-4

Salas, R., Guimerà, J., Mas, R., Martín-Closas, C., Meléndez, A., & Alonso, A. (2001). Evolution of the Mesozoic central Iberian Rift System and its Cainozoic inversion (Iberian Chain). *Mémoires du Museum National d'Histoire Naturelle*, *186*, 145–186.

Seton, M., Müller, R. D., Zahirovic, S., Gaina, C., Torsvik, T., Shephard, G., et al. (2012). Global continental and ocean basin reconstructions since 200 Ma. *Earth-Science Reviews*, *113*(3–4), 212–270. https://doi.org/10.1016/j.earscirev.2012.03.002

Shaw, J., Johnston, S. T., Gutiérrez-Alonso, G., Weil, A. B., Gutiérrez-Alonso, G., & Weil, A. B. (2012). Oroclines of the Variscan orogen of Iberia: Paleocurrent analysis and paleogeographic implications. *Earth and Planetary Science Letters*, *329-330*, 60–70. https://doi.org/10.1016/j.epsl.2012.02.014

Simón Gómez, J.L. (1982). Compresión y distensión alpinas en la Cadena Ibérica oriental, (Tesis Doctoral). Universidad de Zaragoza. 501 pp.

Stampfli, G. M., Hochard, C., Vérard, C., & Wilhem, C. (2013). The formation of Pangea. *Tectonophysics*, *593*, 1–19.

Staub, R. (1926). *Gedanken zur Tektonik Spaniens* (Vol. 71). Zürich. Vierteljahrsschrift der Naturforschenden Gesellschaft.

Tarling, D., & Hrouda, F. (Eds) (1993). *Magnetic anisotropy of rocks*. London: Springer Science & Business Media.

Tauxe, L. (2010). Essentials of paleomagnetism. Retrieved from https://scholar.google.com/scholar?cluster=682416853050055267&hl=en&oi=scholarr#0

Tauxe, L., & Watson, G. S. (1994). The fold test: An eigen analysis approach. *Earth and Planetary Science Letters*, *122*, 331–341.

Torsvik, T. H., van der Voo, R., Preeden, U., Mac Niocaill, C., Steinberger, B., Doubrovine, P. V., et al. (2012). Phanerozoic polar wander, palaeogeography and dynamics. *Earth-Science Reviews*, *114*(3–4), 325–368. https://doi.org/10.1016/j.earscirev.2012.06.007

van der Voo, R. (1990). The reliability of paleomagnetic data. *Tectonophysics*, *184*(1), 1–9.

van Staal, C. R., Whalen, J. B., Valverde-Vaquero, P., Zagorevski, A., & Rogers, N. (2009). Pre-Carboniferous, episodic accretion-related, orogenesis along the Laurentian margin of the northern Appalachians. *Geological Society, London, Special Publications*, *327*(1), 271–316. https://doi.org/10.1144/SP327.13

Veevers, J. J. (2004). Gondwanaland from 650–500 Ma assembly through 320 a merger in Pangea to 185-100 Ma breakup: Supercontinental tectonics via stratigraphy and radiometric dating. *Earth-Science Reviews*, *68*(1–2), 1–132. https://doi.org/10.1016/j.earscirev.2004.05.002

Velzen, A. J., & Zijderveld, J. D. A. (1995). Effects of weathering on single-domain magnetite in Early Pliocene marine marls. *Geophysical Journal International*, *121*(1), 267–278. https://doi.org/10.1111/j.1365-246X.1995.tb03526.x

Villas, E. (1995). Caradoc through early Ashgill brachiopods from the Central-Iberian Zone (Central Spain). *Geobios*, *28*(1), 49–84. https://doi.org/10.1016/S0016-6995(95)80204-5

Vissers, R. L. M., van Hinsbergen, D. J. J., van der Meer, D. G., & Spakman, W. (2016). Cretaceous slab break-off in the Pyrenees: Iberian plate kinematics in paleomagnetic and mantle reference frames. *Gondwana Research*, *34*, 49–59. https://doi.org/10.1016/J.GR.2016.03.006

Weil, A. B., Gutiérrez-Alonso, G., & Conan, J. (2010). New time constraints on lithospheric-scale oroclinal bending of the Ibero-Armorican Arc: A palaeomagnetic study of earliest Permian rocks from Iberia. *Journal of the Geological Society*, *167*(1), 127–143. https://doi.org/10.1144/0016-76492009-002

Weil, A. B., Gutiérrez-Alonso, G., Johnston, S. T., & Pastor-Galán, D. (2013). Kinematic constraints on buckling a lithospheric-scale orocline along the northern margin of Gondwana: A geologic synthesis. *Tectonophysics*, *582*, 25–49. https://doi.org/10.1016/j.tecto.2012.10.006

Weil, A. B., & Yonkee, A. (2009). Anisotropy of magnetic susceptibility in weakly deformed red beds from the Wyoming salient, Sevier thrust belt: Relations to layer-parallel shortening and orogenic curvature. *Lithosphere*, *1*(4), 235–256. https://doi.org/10.1130/L42.1

Zijderveld, J. D. A. (1967). A.C. demagnetization of rocks: Analysis of results. In D. Collinsson, K. Creer, & S. Runcorn (Eds.), *Methods of paleomagnetism*, (pp. 254–286). Amsterdam: Elsevier.